PAPER

Analysis of different conductive pastes to form the contact with the boron back surface field in PERT silicon solar cells

To cite this article: Izete Zanesco *et al* 2019 *Mater. Res. Express* **6** 115535

View the article online for updates and enhancements.

Materials Research Express

PAPER

Analysis of different conductive pastes to form the contact with the boron back surface field in PERT silicon solar cells

Izete Zanesco[1] , Thais Crestani, Adriano Moehlecke and Moussa Ly

Solar Energy Technology Nucleus (NT-Solar), School of Technology, Pontifical Catholic University of Rio Grande do Sul (PUCRS), Porto Alegre, Brazil

[1] Author to whom any correspondence should be addressed.

E-mail: izete@pucrs.br, realthaiscrestani@gmail.com, moehleck@pucrs.br and moussa.ly@pucrs.br

Abstract

The industrial production of solar cells of the PERC family is growing, because the potential to increase the efficiency due to the passivation of the rear face. The PERT solar cell is a cost-effective structure of the PERC configurations. The goal of this paper is to analyze the influence in the electrical parameters of different metal pastes used to form the contact with the boron back surface field of PERT solar cells passivated with silicon dioxide on both sides and developed with a cost-effective process. The boron doped BSF and phosphorus emitter were carried out with reduction of steps. Solar cells were processed with three different conductive pastes: (1) an aluminum paste (PV381), (2) a silver/aluminum paste (PV3N1) and (3) a silver paste (PV51G), with different viscosity and solids content. The pastes were produced by DuPont. The PV381 and PV3N1 pastes produced solar cells with the efficiency of 16.2% and 15.9%, respectively. The higher open circuit voltage was achieved with the aluminum paste, indicating that this paste is more effective to produce the selective back surface field. The PV51G paste is not suitable to form the rear contact.

1. Introduction

The industrial production of silicon solar cells of the PERC (passivated emitter and rear cell) family is growing. The PERC structures, such as PERT (passivated emitter, rear totally-diffused), PERL (passivated emitter, rear locally- doped), PERD (passivated emitter, rear directly-contacted) and PERF (passivated emitter, rear floating-junction) solar cells, are gaining the market share, dominated by the aluminum back surface field (Al-BSF) technology, because the potential of achieving high efficiency [1, 2]. The PERT cell is one structure of the PERC family and can be manufactured with a cost-effective process. The major advantages of the PERC structures are the reduction of the minority charge carrier recombination and the improved reflectance in the rear face, that are limited in the Al-BSF solar cells. The first high efficiency silicon solar cells was developed with PERC structure and the efficiency of 21.8% was obtained in devices with 4 cm^2 and produced with high quality metal grid using photolithography steps. This result was published in 1988 [2], but the concept of PERC structure was proposed in 1983. Currently, different processing techniques and variations of the PERC structure are being studied [3]. The efficiency of the PERC solar cells, produced in monocrystalline silicon wafers, reached the efficiency of 23% in a large area, in contrast with the 18%–19% efficiency of Al-BSF multicrystalline [4].

The PERC family is becoming the new standard to monocrystalline solar cells. The increase of the efficiency causes the decrease in the price of electrical energy produced by photovoltaic modules, if the production cost is kept. Based on this advantage, the market share of the PERC structure may reach 75% in the 2026 [5].

The front emitter of p-type PERC and Al-BSF solar cells are performed with phosphorus diffusion and the silicon nitrite layer passivates the emitter and forms the anti-reflective coating. The SiN_x is usually deposited by plasma-enhanced chemical vapor deposition (PECVD). Then, in the current technology, the phosphorus n$^+$ emitter is well passivated. The main difference between the two solar cell structures is the technology to perform the back surface field and the thin film to passivate the rear face. In the Al-BSF solar cells, the passivation of rear surface is not possible because the formation of the aluminum back surface field with aluminum paste

screen-printed in the whole rear area. However, the passivation of the two surfaces of the crystalline silicon solar cells is important to achieve high efficiency because it reduces the recombination of the minority charge carriers [6, 7]. To passivate the emitter or the BSF a dielectric material can be used [8].

The standard of the solar cell industry is crystalline silicon wafers, dominated by the p-type multicrystalline silicon [9]. Recently, the price of the crystalline silicon wafers grown by the Czochralski method (Si-Cz) declined, becoming the PERC solar cell structures economic competitive [10]. If the back surface field is formed with boron diffusion in p-type wafers, the rear surface can be passivated, in addition to the front emitter. In this case, both sides can be passivated with silicon dioxide, grown simultaneously on the emitter and BSF in the same thermal oxidation. Studies reported that this dielectric is effective to passivate the n^+ and p^+ heavily doped regions [11]. However, in the dry thermal oxidation the growth rate is higher in the phosphorus doped region than in the boron doped region [12]. In previous works were found that a 10 nm layer of SiO_2 is effective to passivate the n^+ emitter [13].

Different techniques can be used to carry out the boron diffusion in silicon wafers. A method used is the deposition of the solution with boron on one surface of the silicon wafer by the spin coating technique and the boron diffusion can be carried out in a quartz tube furnace [14–16]. Solar cells with boron back surface field and passivation of both faces with silicon dioxide reached the efficiency of 16.0%. This value is 0.7% (absolute) higher than the efficiency of the devices without passivation [14]. The boron emitter was also developed by the plasma immersion ion implantation and B_2H_6 to produce n-type PERT solar cells. High open circuit voltage of 695 mV was achieved. After the annealing process, solar cells presented the efficiency of 19.8% [17]. Techniques with laser radiation allow to produce the doping profile accurately by adjusting the laser parameters and selecting an appropriate doping source. For instance, the rear surface passivation and contact can be produced with a stack of Al_2O_3/SiN_x, laser ablation and screen-printed aluminium paste, forming the local back surface field. Industrial solar cells achieved an efficiency higher than 20% [18, 19].

The application of a tunnel oxide layer to passivate the contacts improves the efficiency. A tunnel oxide layer less than 2 nm thick improved the open circuit voltage [20]. The quality of the passivation is associated with the physical properties of the thin layer and is influenced by the annealing. Different methods are used to grow the thin tunnel layer, but the thermally grown oxide leads to a high quality passivation [21].

One challenge is the contact formation in the p^+ substrate, through the dielectric layer. PERC solar cells are usually produced opening the passivation coating by laser. Studies of the contact or BSF formation between the screen-printed Al paste and Si substrate have been reported and explained by the diffusion of Si in Al [22]. Aluminum particles melt during the firing process and start to alloy with the Si substrate. At temperatures above the eutectic point, Si from the substrate diffuses into the Al paste [23]. The peak firing temperature affects the p^+ thickness. If a dielectric coating is formed to passivate the p^+ surface, the Al paste may not fire through the passivation layer [24].

The p^+ heavily doped region contacted with silver paste results in a high contact resistivity. Then, Al is added to the Ag paste in order to reduce the contact resistivity, but the resistivity of the metal finger and the minority charge carrier recombination in the surface increase [25]. Specifically, Al is added to the Ag conductive paste to increase the contact points. The contact resistivity may be reduced about three orders of magnitude, because the silver/aluminum paste creates large and deep metal spikes [26, 27]. If a high amount of Al is added to the Ag paste, the leakage currents of the solar cell increases due to large Al spikes [28]. The particle size of the aluminum powder affects the contact resistivity, which decreases with the increasing of Al particle size [26]. Wu *et al* [27] reported a microstructural study of the contact of the Ag/Al conductive paste with boron doped emitters, that indicated the formation of microscale metallic spikes of Al-Ag alloy and nanoscale metallic spikes of Ag-Si alloy, that allow the direct contact to the emitter.

The process to manufacture the PERC solar cell structures must be cost-effective and the approaches to produce the BSF and the passivation of surfaces, combined with the rear contact formation, affect the efficiency and the production cost. Then, the conductive paste used to form the contact with the SiO_2 passivated boron BSF affects the electrical parameters of the solar cells. Based on these facts, the goal of this paper is to analyse the influence in the electrical parameters of different metal pastes used to form the contact with the boron back surface field of cost-effective PERT solar cells, directly through the thin SiO_2 passivation layer. The boron doped BSF and phosphorus emitter were carried out with reduction of steps, based on the patent BR1020120306069 [29] and the process is easily adapted to the current industry of solar cells. A silicon dioxide layer was grown on the emitter and BSF to passivate the surfaces and, during the firing step, the conductive paste screen-printed over the thin silicon dioxide layer contacts the boron doped BSF.

2. Materials and methods

The developed PERT solar cell is illustrated in figure 1. The p^+ BSF was doped with boron and the n^+ emitter was formed by the phosphorus diffusion. The surface passivation was implemented with the growth of a SiO_2 layer.

Figure 1. Schematic drawing of the PERT solar cell with boron BSF.
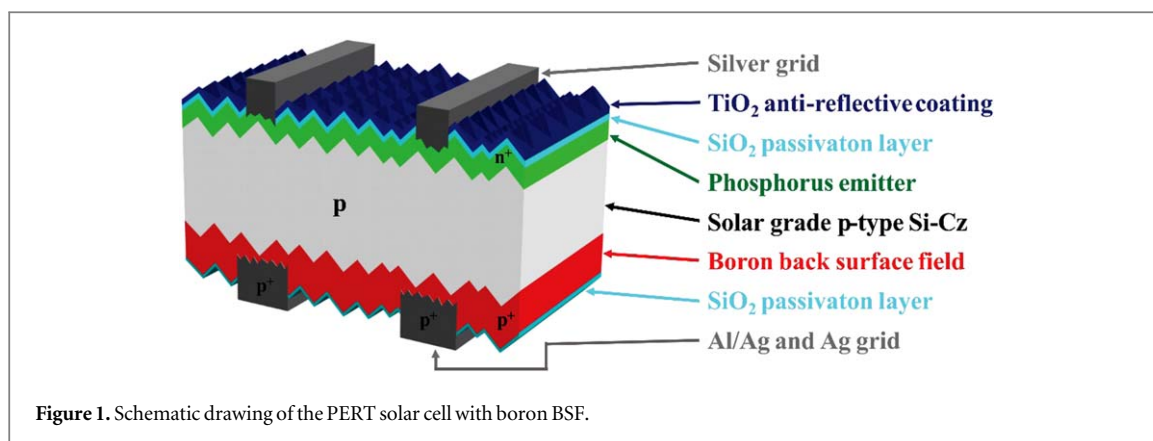
Figure 2 summarizes the process sequence of the PERT silicon solar cells with reduction of thermal and cleaning steps. Solar grade p-type Si-Cz wafers with 100 mm diameter, thickness of (200 ± 30) μm, orientation of the lattice planes {100} and resistivity from 1 Ω.cm to 20 Ω.cm were used. Firstly, the silicon wafers were textured in a solution of KOH, isopropyl alcohol and deionized water and, then, were processed in the RCA wet-chemical cleaning [30]. The wafers were rinsed with deionized water after each chemical step. The solution with boron (PBF20 from Filmtronics) was deposited by the spin coating method and, after evaporation of the solvents, the wafers were introduced into the quartz tube furnace to diffuse boron to form the back surface field at the temperature of 970 °C [31, 32]. In the same thermal step, the oxidation was performed to protect the boron doped face from phosphorus diffusion. In the next steps, the silicon dioxide on the face where phosphorus will be diffused was etched in a solution with hydrofluoric acid and the silicon wafers were cleaned in the RCA solution. This process was based on the patent BR1020120306069 [29] and two thermal steps and one wet chemical cleaning were avoided, if the process is compared to the typical boron diffusion with BBr$_3$. The diffusion of phosphorus to form the n$^+$ emitter was implemented with POCl$_3$. Afterwards, the boron and phosphorus silicates grown during the diffusions were etched and the RCA chemical cleaning prepared the silicon wafer to the dry oxidation to passivate the surfaces. The SiO$_2$ layer thickness in the phosphorus emitter was of approximately 10 nm [13]. The sheet resistance of the phosphorus emitter and boron BSF was measured, after the growth of SiO$_2$ to passivate the surfaces, in a sample of each diffusion process, in 13 regions of the silicon wafer. The doping profile was also measured by ECV (electrochemical capacitance-voltage) technique.

The 60 nm thick titanium dioxide anti-reflective (AR) coating was deposited on the front face by electron-beam physical vapor deposition. In the last step, the metal grid was screen-printed on the front and on the rear face. The PV17F silver paste, produced by Dupont, was deposited on the phosphorus emitter. This paste was developed to form the electrical contact in the n$^+$ region and to allow the soldering of solar cells. The silver paste is free of cadmium. Figure 3 shows the Ag paste finger formed on the front face, with a width of approximately 110 μm and a height of around 34 μm. The metal grid covered about. 7% of the front surface.

On the rear face, a metal grid was also screen-printed. The area covered with metal grid was 14.3%. Three different pastes were used: (1) an aluminum paste, named PV381, (2) a silver/aluminum paste, named PV3N1 and (3) the silver paste, denominated PV51G. The three pastes are produced by DuPont. The solids content of the aluminum, aluminum/silver and silver paste are around 60%, 90% and 50%, respectively. In the PV3N1 paste, the aluminum content is less than 10%. The viscosity of the paste increases with solid phase volume and must be sufficiently low during printing to produce continuous lines. Another important feature of the conductive paste is to form a metal finger with high height-to-width ratio.

The PV381 aluminum paste is used to form the homogeneous back surface field by the current industry of Al-BSF solar cells. Important features of this paste are to produce a low bow of the silicon wafer and an effective BSF. The PV3N1 conductive paste has about three times higher viscosity and around twice solids content than PV51G paste. The silver content in the Ag/Al paste is around 60% higher than in the silver paste. The PV3N1 silver/aluminum paste was developed to produce the contact in the boron emitter formed in n-type silicon wafer, with the property of perforating the passivation and/or the anti-reflective layer. The Ag/Al paste produces low contact resistivity, low gridline resistivity and has a solderable silver composition. The PV51G silver paste is used to produce the busbar for soldering the solar cells when the aluminum paste is used to form the homogeneous Al-BSF. This paste has high conductivity and a specific silver composition that enables the soldering of solar cells to manufacture the photovoltaic module.

The firing process is one of the key steps with which the metal contact is formed in a silicon solar cell. After the drying of the conductive pastes screen-printed independently on the front and rear face, the pastes were fired simultaneously in the belt furnace. The firing temperature (T$_F$) was experimentally optimized to produce the

Figure 2. Process sequence to produce the boron doped PERT solar cells with reduction of thermal and chemical steps.

Figure 3. Finger produced with the PV17F silver paste on the n^+ emitter. The width and height of the finger are approximately 110 μm and 34 μm, respectively. Image obtained in the optical microscope.
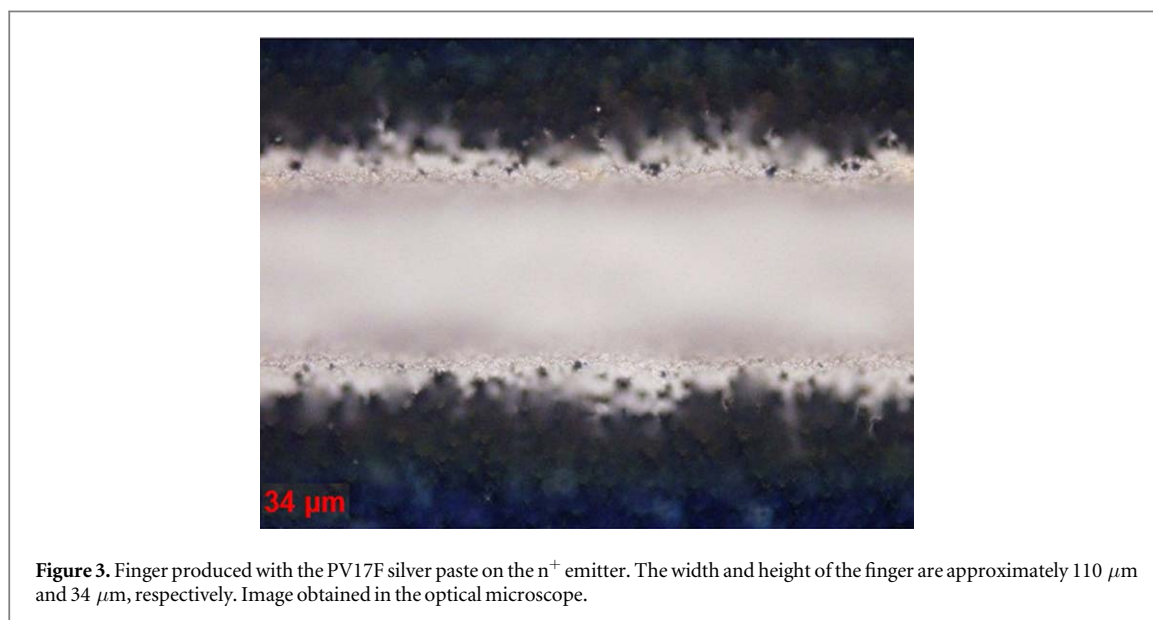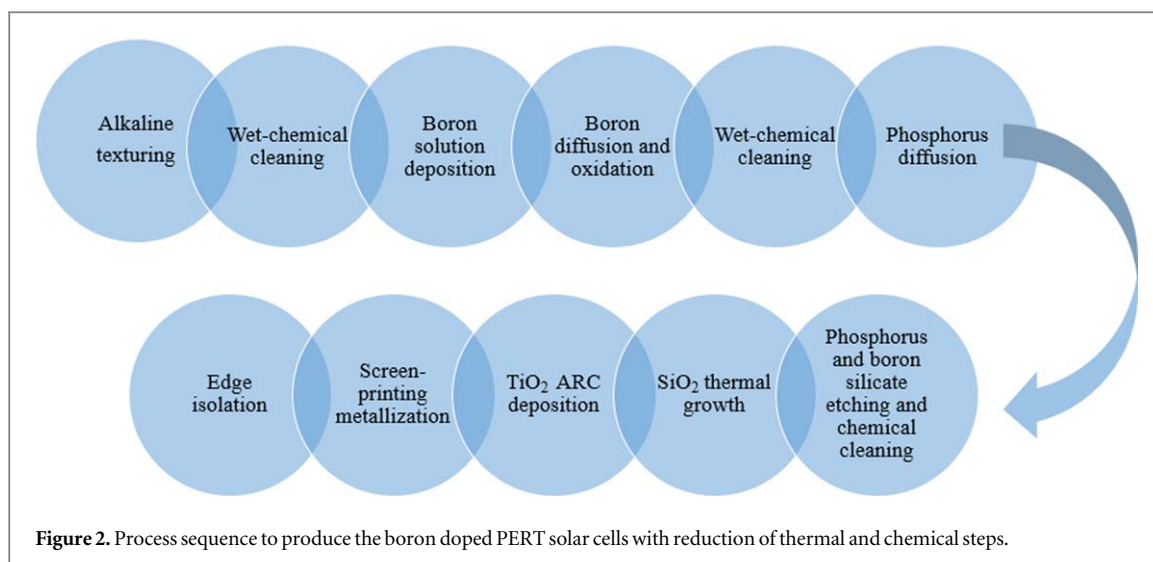
contact with the p^+ substrate through the thin SiO_2 surface passivation layer. Therefore, the firing temperature was ranged from 840 °C to 920 °C for solar cells with the PV381 paste and from 800 °C to 890 °C for the PV3N1 paste. For solar cells with PV51G paste, the T_F was ranged from 850 °C to 890 °C. By this process and the Al and Ag/Al pastes, an aluminum and boron selective BSF can be produced in PERT solar cells.

The solar cells with area of 61.58 cm^2 and a standard two busbar grid were characterized measuring the current density as a function of applied voltage (curve J-V) using a solar simulator under standard conditions: solar cell temperature of 25 °C, irradiance of 1000 W m^{-2} and standard solar spectrum AM1.5. Then, the short-circuit current density (J_{SC}), the open circuit voltage (V_{OC}), the fill factor (FF) and the efficiency (η) of the solar cells were compared. The metal fingers on the rear face with the Ag, Al and Ag/Al pastes were evaluated with an optical microscope and the height and width of the fingers were estimated.

3. Results and discussions

3.1. Sheet resistance and doping profile

The sheet resistance in a sample of each process was measured after the oxidation process to passivate both surfaces of the solar cells. Table 1 shows the average value and standard deviation of the sheet resistance measured in the front phosphorus emitter ($R\square_P$) and in the boron back surface field ($R\square_B$). The average sheet resistance of the boron and phosphorus heavily doped region was $(45.1 \pm 1.9)\,\Omega/\square$ and $(59 \pm 5)\,\Omega/\square$, respectively. The boron diffusion was more homogeneous, since the standard deviation is smaller.

The boron and phosphorus profiles measured by ECV technique are presented in the figure 4. The junction depth (x_j) of the n^+ emitter was about 0.37 μm. However, the junction depth of the boron BSF is deeper than the emitter, being around 0.90 μm. The surface concentration (C_S) of boron increases from 3.8 $\times$ 10^{19} atoms/cm^3 to 1.8 $\times$ 10^{20} atoms/cm^3 when the depth is 0.15 μm, as figure 4 shows. This behavior of boron profile was also observed with diffusion using BBr$_3$ and performed in n-type silicon wafers and the sheet resistance was in the range of 60–70 $\Omega/\square$ [33, 34].

On the other hand, the C_S found in the phosphorus profile was 1.4 $\times$ 10^{21} atoms/cm^3, typical of phosphorus diffusion with POCl$_3$ [34]. In this process, the oxidation to shield the face doped with boron to the phosphorus diffusion, was carried out in the same thermal step that boron diffusion and boron segregated to silicate layer during the oxidation [35]. In this case, the typical values of boron surface concentration are around 3 $\times$ 10^{19}–5 $\times$ 10^{19} atoms/cm^3 [35].

3.2. Comparison of the fingers of the rear metal grid

The figure 5 compares the fingers of the metal grid screen-printed on the boron BSF using the different pastes and the same screen mask. The finger formed with the PV51G silver paste is shown in figure 5(a) and has a height of approximately 7 μm and a width of 315 μm. Figure 5(b) shows the finger obtained with PV381 aluminum paste. The height is 15 μm and the width is 320 μm. With the aluminum paste, the height is around twice the height of the finger produced with PV51G silver paste, meanwhile the width of the finger is similar. The PV3N1 silver/aluminum paste produced the best finger, with greater height and smaller width, as figure 5(c) presents. The height and width of the finger were of about of 20 μm and 170 μm, respectively. This paste produced a residue of the material in the region close to the fingers that can increase the minority charge carrier recombination in this area. The great height-to-width ratio of the finger produce with the PV3N1 paste is related to the higher viscosity of this paste.

3.3. Analysis of the electrical parameters of the solar cells

The table 2 shows the average electrical parameters of the PERT solar cells produced with the three conductive pastes as a function of the firing temperature. With the PV51G silver paste, the average efficiency of (10.2 $\pm$ 0.2)% was obtained for the firing temperature of 860 $^\circ$C. The fill factor was low, with values $\leqslant$0.5, for all firing temperatures, and the fill factor affected the efficiency of the solar cells. This result was caused by the high contact resistivity of the Ag paste and resistance of the metal finger on the rear face that presented low height, leading to a high series resistance. The average open circuit voltage decreased with the increase of the firing temperature. The higher average open circuit voltage occurred for the lower firing temperature and the average V_{OC} of 592 mV was obtained for this firing temperature.

The average efficiency of (15.9 $\pm$ 0.4)% was achieved with the solar cells manufactured with the PV381 aluminum paste fired at temperature of 860 $^\circ$C. For all the firing temperatures, the fill factor was higher than that obtained with the PV51G paste. In this case, the open circuit voltage also tends to decrease with the increasing of firing temperature. With the aluminum paste, the highest average open circuit voltage was 600.2 mV, 8 mV, higher than that obtained with the PV51G paste, indicating that the aluminum paste reduced the minority charge carrier recombination in the region with the metal grid and/or produced an effective selective BSF.

The solar cells developed with PV3N1 silver/aluminum paste presented the average efficiency of (15.8 $\pm$ 0.2)% with the firing temperature in the range of 850 $^\circ$C to 860 $^\circ$C, similar to the efficiency achieved with the aluminum paste. Firing temperatures lower than or equal to 820 $^\circ$C did not form a suitable electrical contact. In this case, the series resistance is high and, consequently, the fill factor is low. Like the PV51G and PV381, the open circuit voltage tends to decrease with the increase of the firing temperature, as figure 6(a) shows. The paste with silver/aluminum resulted in an average open circuit voltage lower than that obtained with the aluminum paste because the presence of silver in the formation of the selective BSF. For the firing temperature of 860 $^\circ$C, the average open circuit voltage of solar cells screen-printed with the PV51G, PV381 and PV3N1 pastes was 585.2 mV, 597.5 mV and 593.5 mV, respectively. This result indicates that the presence of Al in the conductive paste produced a selective BSF. The V_{OC} of solar cells produced with the Ag and Ag/Al conductive pastes is more affected by the firing temperature, due to the presence of silver, that increases the minority charge carrier recombination. In this case, the V_{OC} of the solar cells screen-printed with the silver paste is more reduced than that of the devices with Ag/Al paste by the increasing of T_F, in spite of the less silver content.

The average values of the fill factor of the PERT solar cells with rear grid formed with the PV51G, PV381 and PV3N1 pastes as a function of the firing temperature are compared in figure 6(b). For T_F higher than 840 $^\circ$C, the fill factor of the solar cells screen-printed with the PV381 and PV3N1 pastes is similar and was not influenced by the firing temperature in the range of 860 $^\circ$C to 900 $^\circ$C. Meanwhile the values obtained with the PV51G paste are low due to the high series resistance caused by the low height of the metal fingers and the contact resistance. For T_F = 860 $^\circ$C, the average fill factor for PV51G paste was 0.513 while for PV381 and PV3N1 the values were 0.791
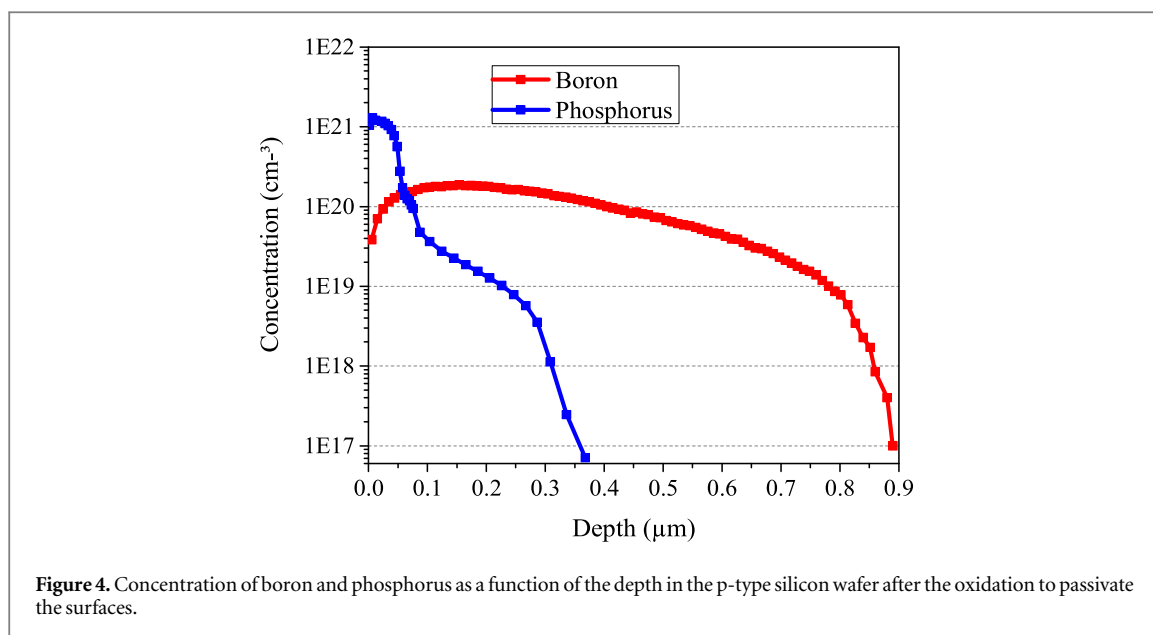
Figure 4. Concentration of boron and phosphorus as a function of the depth in the p-type silicon wafer after the oxidation to passivate the surfaces.

Table 1. Average sheet resistance of the phosphorus emitter ($R\square_P$) and of the boron back surface field ($R\square_B$).

Paste	$R\square_B (\Omega/\square)$	$R\square_P(\Omega/\square)$
PV51G	50.8 ± 2.8	63 ± 6
PV381	42.2 ± 1.6	58 ± 5
PV3N1	42.2 ± 2.0	57 ± 7
Average	45.1 ± 1.9	59 ± 5

and 0.784, respectively. This result indicates that the contact resistance was similar to the Al and Ag/Al paste, in spite of the presence of silver in the latter paste. The figure 6(c) shows that the short-circuit current density was practically unaffected by the T_F for temperatures higher than 840 °C. In this firing temperature range, the average value was 33.3 mA cm^{-12} for the aluminum paste, and 33.9–34.0 mA cm^{-12} for the two pastes with silver content. The short-circuit current is low at $T_F \leqslant 820$ °C because the firing temperature did not produce suitable electrical contact between the metal paste and the substrate and the contact resistance is high. This result affects the efficiency of the devices, as figure 6(d) illustrates. The efficiency was influenced by the fill factor as figures 6(b) and (d) show. For $T_F = 860$ °C, the average efficiency of the PERT solar cell with the PV51G paste was 10.2%, meanwhile the values of the solar cells screen-printed with the PV381 and PV3N1 pastes were similar, of 15.9% and 15.8%, respectively. The devices with the PV381 paste presented higher V_{OC} and those with the PV3N1 paste shown a slightly high short-circuit current density.

3.4. Comparison of the solar cell with high efficiency

The table 3 presents the electrical parameters of the solar cells with the highest efficiency as a function of firing temperature. For the three conductive pastes, the firing temperature of 860 °C resulted in higher efficiency and the solar cells manufactured with the aluminum paste achieved the efficiency of 16.2% and the fill factor of 0.807. The efficiency of 15.9% was obtained with the PV3N1 silver/aluminum paste.

The J-V curve of solar cells as a function of firing temperature for the different metal pastes are compared in figure 7. The decreasing of the open circuit voltage with the increasing of the firing temperature was confirmed for the three conductive pastes. Figure 7(a) indicates that the low fill factor obtained with the PV51G paste is related to the series resistance of the solar cells. Then, this paste is not suitable to produce PERT solar cells. The solar cells manufactured with the aluminum paste presented similar J-V curves in the range of firing temperature from 840 °C to 900 °C. In this range of T_F, the same conclusion is obtained for the PV3N1 paste. However, the firing temperature lower than 840 °C produced a high contact resistance.

Comparing the solar cell screen-printed with the PV381 aluminum paste and PV3N1 silver/aluminum paste fired at $T_F = 860$ °C, we observed that the V_{OC} obtained with the aluminum paste is slightly higher than that

Figure 5. Finger of the metal grid screen-printed on the boron BSF evaluated in the optical microscope and formed with the (a) PV51G Ag paste (height 7 μm and width 314 μm), (b) PV381 Al paste (height 15 μm and width 320 μm) and (c) PV3N1 Ag/Al paste (height 19 μm and 168 μm width). The same screen mask was used.
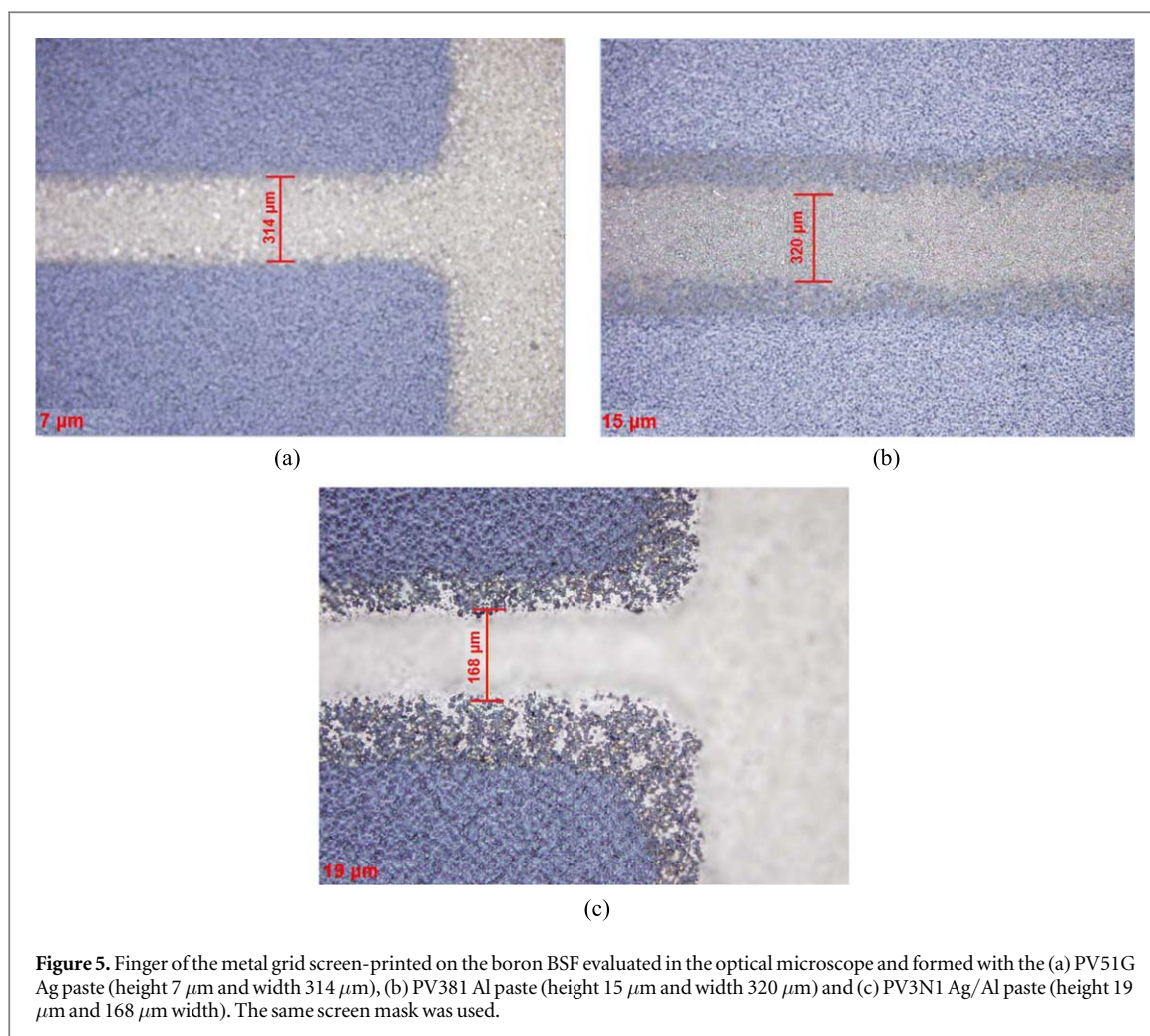
Table 2. Average open circuit voltage (V_{OC}), short-circuit current density (J_{SC}), fill factor (FF) and efficiency (η) of the PERT solar cells developed with different conductive pastes screen-printed on the boron BSF as a function of the firing temperature (T_F).

Paste	Number of cells	T_F (°C)	V_{OC} (mV)	J_{SC} (mA cm^{-2})	FF	η (%)
PV51G	3	850	592 $\pm$ 4	33.9 $\pm$ 0.2	0.494 $\pm$ 0.029	9.9 $\pm$ 0.5
	4	860	585.2 $\pm$ 1.6	33.9 $\pm$ 0.2	0.513 $\pm$ 0.010	10.2 $\pm$ 0.2
	4	870	579 $\pm$ 4	33.8 $\pm$ 0.1	0.493 $\pm$ 0.008	9.7 $\pm$ 0.2
	3	880	576.1 $\pm$ 2.2	33.8 $\pm$ 0.1	0.489 $\pm$ 0.008	9.6 $\pm$ 0.2
	3	890	566.7 $\pm$ 2.9	33.9 $\pm$ 0.1	0.457 $\pm$ 0.010	8.8 $\pm$ 0.2
PV381	3	840	600.2 $\pm$ 0.5	33.7 $\pm$ 0.1	0.754 $\pm$ 0.018	15.3 $\pm$ 0.4
	2	860	597.6 $\pm$ 1.3	33.7 $\pm$ 0.2	0.791 $\pm$ 0.023	15.9 $\pm$ 0.4
	2	880	597.6 $\pm$ 1.8	33.3 $\pm$ 0.6	0.796 $\pm$ 0.025	15.8 $\pm$ 0.2
	2	900	592.7 $\pm$ 1.5	33.8 $\pm$ 0.4	0.79 $\pm$ 0.03	15.8 $\pm$ 0.5
	2	920	590.9 $\pm$ 1.2	33.7	0.778 $\pm$ 0.004	15.5 $\pm$ 0.1
PV3N1	3	800	601 $\pm$ 3	25 $\pm$ 4	0.41 $\pm$ 0.04	6.2 $\pm$ 1.6
	3	820	601.0 $\pm$ 0.3	33.1 $\pm$ 0.4	0.545 $\pm$ 0.006	10.8 $\pm$ 0.2
	3	840	597.1 $\pm$ 0.3	33.7 $\pm$ 0.2	0.766 $\pm$ 0.012	15.4 $\pm$ 0.2
	3	850	590 $\pm$ 3	33.8 $\pm$ 0.1	0.791 $\pm$ 0.001	15.8 $\pm$ 0.2
	3	860	593.5 $\pm$ 0.9	33.9 $\pm$ 0.1	0.784 $\pm$ 0.010	15.8 $\pm$ 0.2
	3	870	585.5 $\pm$ 1.5	34.0 $\pm$ 0.1	0.784 $\pm$ 0.010	15.6 $\pm$ 0.2
	3	880	585 $\pm$ 10	33.7 $\pm$ 0.5	0.779 $\pm$ 0.013	15.4 $\pm$ 0.6
	3	890	576 $\pm$ 4	33.9 $\pm$ 0.1	0.787 $\pm$ 0.016	15.4 $\pm$ 0.2

found with the silver/aluminum paste. The difference in V_{OC} of the devices is 4 mV, indicating that the aluminum paste is more effective to form the selective back surface field. The lower V_{OC} of the solar cell with the PV3N1 paste is probably due to the presence of silver that increases the recombination in the region heavily

Figure 6. Average values of the (a) open circuit voltage, (b) short-circuit current density, (c) fill factor and (d) efficiency of the solar cells as a function of the firing temperature for different conductive pastes screen-printed on the boron BSF.
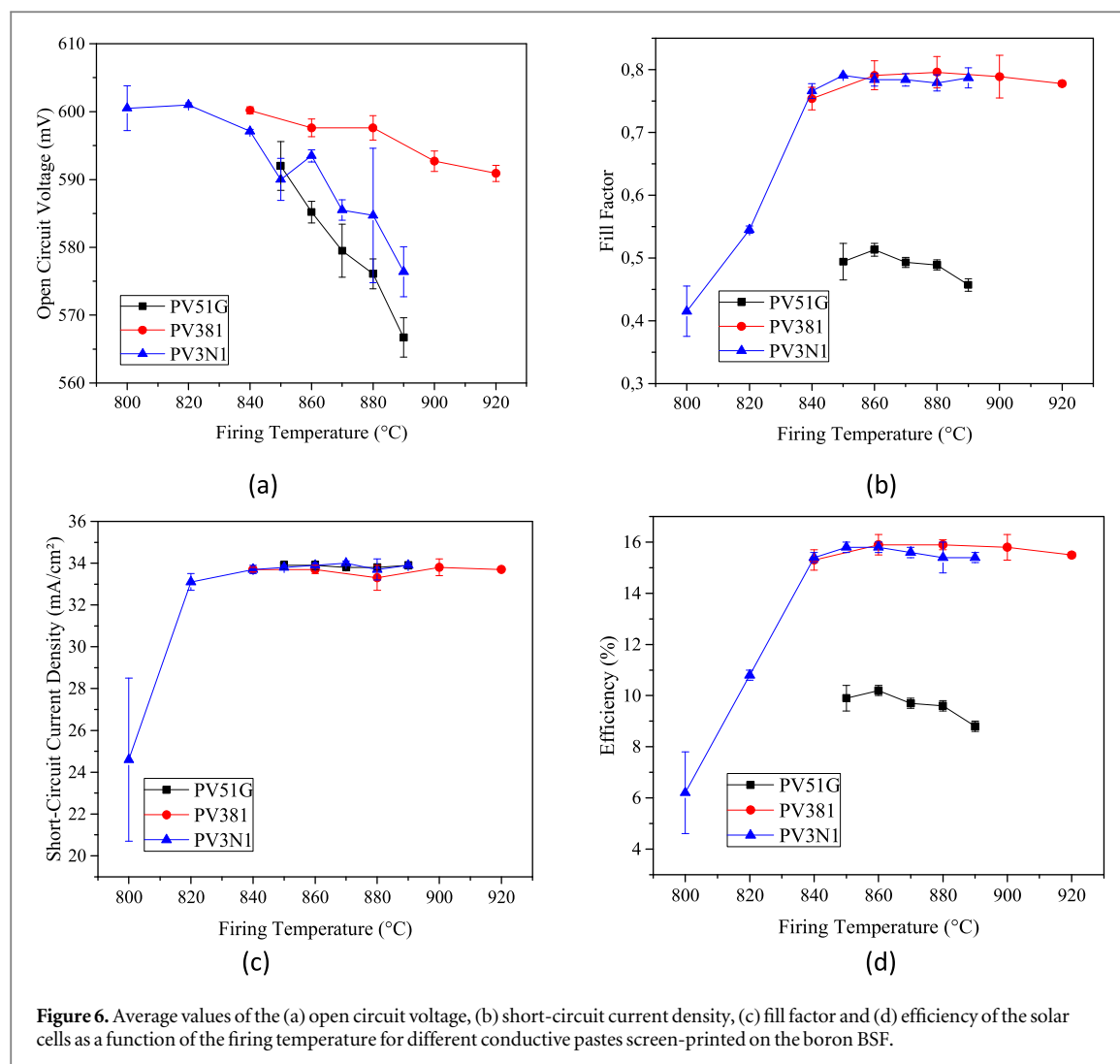
Table 3. Electrical parameters of the PERT solar cell with the highest efficiency and screen-printed with the three conductive pastes as a function of the firing temperature.

Paste	Cell	T_F (°C)	V_{OC} (mV)	J_{SC} (mA cm^{-2})	FF	η (%)
PV51G	2	850	593.8	33.9	0.505	10.2
	4	860	586.4	33.8	0.527	10.4
	8	870	583.8	33.8	0.503	9.9
	14	880	578.3	33.8	0.496	9.7
	16	890	569.6	33.9	0.467	9.0
PV381	4	840	600.2	33.8	0.757	15.4
	5	860	598.5	33.5	0.807	16.2
	9	880	598.9	32.9	0.814	16.0
	14	900	591.7	33.6	0.813	16.1
	16	920	590.0	33.7	0.780	15.5
PV3N1	3	800	602.0	28.8	0.457	7.9
	6	820	600.9	33.4	0.550	11.0
	11	840	597.0	33.6	0.780	15.7
	3	850	592.2	33.8	0.792	15.9
	15	860	594.5	33.7	0.795	15.9
	12	870	584.6	33.8	0.797	15.7
	17	880	591.9	33.8	0.794	15.9
	18	890	574.4	33.7	0.802	15.5

doped with aluminum of the selective back surface field. On the other hand, the solar cell with the silver/aluminum paste produced the $J_{SC} = 33.7$ mA cm^{-2}, which is slightly higher than the J_{SC} obtained with the aluminum paste, of 33.5 mA cm^{-2}. The fill factor was similar.
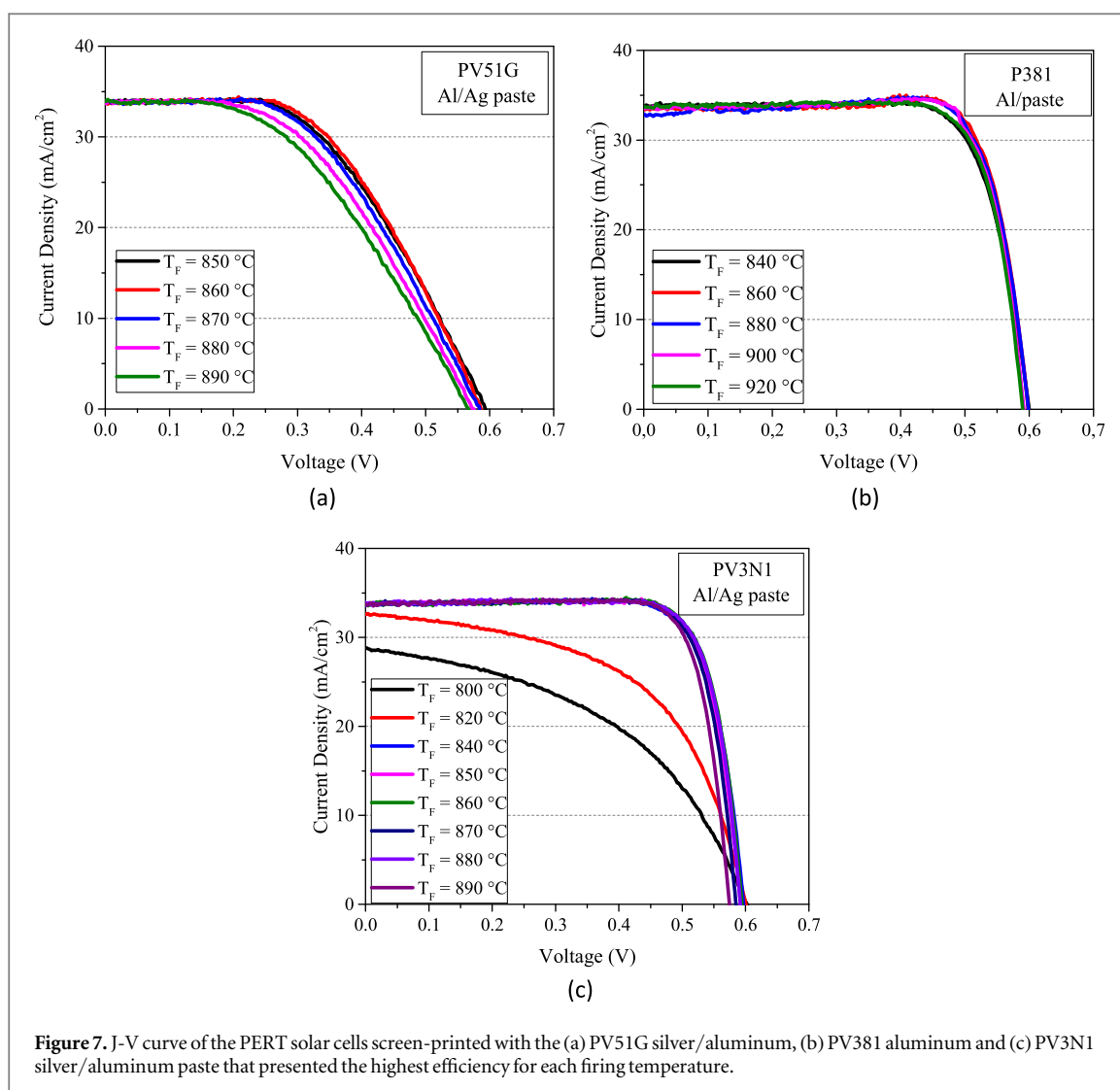
Figure 7. J-V curve of the PERT solar cells screen-printed with the (a) PV51G silver/aluminum, (b) PV381 aluminum and (c) PV3N1 silver/aluminum paste that presented the highest efficiency for each firing temperature.

4. Conclusion

The influence of three different metal pastes to contact the boron back surface field was analyzed: (1) the aluminum paste, denominated PV381, (2) the silver/aluminum paste, named PV3N1 and the silver paste, named PV51G. The PV3N1 Ag/Al paste has higher viscosity than PV51G Ag paste. The height of the fingers of the metal grid was about 7 μm, 15 μm and 20 μm for the PV51G, PV381 and PV3N1 paste, respectively. The reduced height of the finger formed with the PV51G paste is associated to the lower viscosity. The width of the fingers formed with PV51G and PV381 pastes was similar meanwhile the PV3N1 Al/Ag paste produced the best finger, higher and narrower, with a width of 170 μm. For the three evaluated metal pastes the firing temperature of 860 °C produced the PERT solar cells with higher efficiency and the open circuit voltage decreased with the increasing of firing temperature.

The PV51G silver paste produced solar cells with low fill factor, of about 0.5, caused by the high series resistance. The fill factor achieved with the other two conductive pastes was of around 0.80, indicating that the contact resistance was similar to the Al and Ag/Al paste. The average efficiency found with the PV381 aluminum paste was (15.9 $\pm$ 0.4)% and the highest efficiency was 16.2%. The PV3N1 silver/aluminum paste resulted in similar average efficiency of (15.8 $\pm$ 0.2)%.

The aluminum paste produced solar cells with higher V_{OC}, indicating that aluminum paste is more effective to form the selective back surface field. The short-circuit current density was slightly affected by the type of metal paste used. The average value was 33.7 mA cm^{-2}, for the aluminum paste, and 33.9 mA cm^{-2} for the silver and silver/aluminum pastes.

With the aluminum paste a slightly higher average efficiency was obtained, but the screen-printing process must be carried out in two steps, since it is necessary to form the busbar in the rear metal grid with silver/aluminium paste to enable soldering the solar cell, increasing the production cost.

Acknowledgments

ORCID iDs

Izete Zanesco ⓘ https://orcid.org/0000-0003-0823-7806
Adriano Moehlecke ⓘ https://orcid.org/0000-0001-6616-2473

References

[1] Green M 2016 Commercial progress and challenges for photovoltaics *Nature Energy* **1** 15015

[2] Green M A 2015 The passivated emitter and rear cell (PERC): from conception to mass production *Solar Energy Materials & Solar Cells* **143** 190–7

[3] Blakers A 2019 Development of the PERC solar cell *IEEE Journal of Photovoltaics* **9** 629–35

[4] Liu J, Yao Y, Xiao S and Gu G 2018 Review of status developments of high-efficiency crystalline silicon solar cells *J. Phys. D: Appl. Phys.* **51** 1–12

[5] ITRPV 2018 Results 2019 *International technology Roadmap for Photovoltaic* 10th edn (Frankfurt: VDMA) www.itrpv.vdma.org

[6] Rahman M Z and Khan S I 2012 Advances in surface passivation of c-Si solar cells *Materials for Renewable and Sustainable Energy* **1** 1–11

[7] Qiu Y, Wang L, Hao H, Shi W and Lu M 2015 A synergetic effect of surface texture and field-effect passivation on improving Si solar cell performance *Physica* E **71** 96–100

[8] Battaglia C, Cuevas A and Wolf S D 2016 High-efficiency crystalline silicon solar cells: status and perspectives *Energy Enviroment Science* **9** 1552–76

[9] Burger B *et al* 2019 Photovoltaic Report Fraunhofer Institute for Solar Energy Systems and PSE Conferences & Consulting GmbH (www.ise.fraunhofer.de/content/dam/ise/de/documents/publications/studies/Photovoltaics-Report.pdf)

[10] Kumar A, Bieri M, Reindl T and Aberle A G 2017 Economic viability analysis of silicon solar cell manufacturing: Al-BSF versus PERC *Energy Procedia* **130** 43–9

[11] Glunz S W and Feldmann F 2018 SiO$_2$ surface passivation layers—a key technology for silicon solar cells *Sol. Energy Mater. Sol. Cells* **185** 260–9

[12] Ho C P and Plummer J D 1979 Si/SiO$_2$ interface oxidation kinetics: a physical model for the influence of high substrate doping levels *J. Electrochem. Soc.* **126** 1523–30

[13] Zanesco I and Moehlecke A 2015 Analysis of the silicon dioxide passivation and forming gas annealing in silicon solar cells *Solar World Congress* (Daegu, South Korean: International Solar Energy Society) 1–9

[14] Crestani T, Zanesco I and Moehlecke A 2017 Influence of passivation on silicon solar cells with selective back surface field of aluminum and boron *Technology in Metallurgy, Materials and Mining* **14** 1–10

[15] Sun X, Zhao H, Yuan X, Tong H and Yang Y 2019 Spin-on boron diffusion for n-type silicon wafers using borate esters of D-mannitol *Mater. Res. Express* **6** 086307

[16] Ryu K, Cho E, Rohatgi A and Ok Y W 2016 Process development and comparison of various boron emitter technologies for high-efficiency (~21%) n-type silicon solar cells *Prog. Photovoltaics Res. Appl.* **24** 1109–15

[17] Lerata J F, Desruesa T, Percheca J L, Coigb M, Milesib F, Mazenb F, Michelc T, Rouxc L, Veschettia Y and Duboisa S 2016 Boron emitter formation by plasma immersion ion implantation in n-type PERT silicon solar cells *Energy Procedia* **92** 697–701

[18] Huang H *et al* 2017 20.8% industrial PERC solar cell: ALD Al$_2$O$_3$ rear surface passivation, efficiency loss mechanisms analysis and roadmap to 24% *Solar Energy Materials & Solar Cells* **161** 14–30

[19] Werner S *et al* 2017 Key aspects for fabrication of p-type Cz-Si PERC solar cells exceeding 22% conversion efficiency *33rd European PV Solar Energy Conf. and Exhibition (September 2017) (Amsterdam The Netherlands* pp 24–9

[20] Kim H *et al* 2017 Passivation properties of tunnel oxide layer in passivated contact silicon solar cells *Appl. Surf. Sci.* **409** 140–8

[21] Vosse R, Feldmann F, Moldovan A and Hermle M 2018 Comparative study of differently grown tunnel oxides for p-type passivating contacts *Energy Procedia* 124, 448–54

[22] Riegel S, Mutter F, Lauermann T, Terheiden B and Hahn G 2012 Review on screen printed metallization on p-type silicon *Energy Procedia* **21** 14–23

[23] Urrejola E, Peter K, Plagwitz H and Schubert G 2010 Al-Si alloy formation in narrow p-type Si contact areas for rear passivated solar cells *J. Appl. Phys.* **107** 1–5

[24] Rauer M, Schmiga C, Woehl R, Rühle K, Hermle M, Hörteis M, Biro D and Glunz W 2011 Investigation of aluminum-alloyed local contacts for rear surface-passivated silicon solar cells *In: IEEE Journal of Photovoltaics* **1** 22–8

[25] Fritz S, König M, Riegel S, Herguth A, Hörteis M H and Hahn G 2015 Formation of Ag/Al screen-printing contacts on B emitters *In: IEEE Journal of Photovoltaics* **5** 145–51

[26] Aoyama T, Aoki M, Sumita I and Ogura A 2018 Effects of particle size of aluminum powder in silver/aluminum paste on n-type solar cells *AIMS Materials Science* **5** 614–23

[27] Wu W, Roelofs K E, Subramoney S, Lloyd K and Zhang L 2017 Role of aluminum in silver paste contact to boron-doped silicon emitters *AIP Adv.* **7** 015306

[28] Lago R, Pérez L, Kerp H, Freire I, Hoces I, Azkona N, Recart F and Jimeno J C 2010 Screen printing metallization of boron emitters *Prog. Photovoltaics Res. Appl.* **18** 20–7

[29] Zanesco I and Moehlecke A 2012 Impurity diffusion process in silicon wafers to fabricate solar cells (Process of diffusion of dopants in silicon wafers to manufacture solar cells) *Brazilian Patent* PI12030606, BR 10 2012 030606 9

[30] Kern W 1993 *Handbook of Semiconductor Wafer Cleanning Technology* (New Jersey: Noyes Publications)

[31] Crestani T, Zanesco I, Moehlecke A, Razera R A Z, Aquino J, Model J C M and Ly M 2016 Development of the selective back surface field of aluminum and boron in silicon solar cells *Revista Brasileira de Energia Solar* **8** 59–66 (https://rbens.emnuvens.com.br/rbens/issue/view/20)

[32] Crestani T, Zanesco I, Moehlecke A and Ly M 2018 Analysis of the boron concentration profile to produce p-type silicon solar cells by reducing thermal steps *Actas de la XLI Reunión de Trabajo de la Asociación Argentina de Energías Renovables y Medio Ambiente* **6** 159–70

[33] Mojrová B, Comparotto C, Kopecek R and Mihailetchi V D 2016 Optimization of boron diffusion for screen printed n-PERT solar cells *Energy Procedia* **92** 474–8

[34] Komatsu Y, Vlooswijk A H G, Venema P R and Romijn I G 2014 The potencial advange of industrially processed boron emitters compared to phosphorus emitters *Energy Procedia* **55** 241–6

[35] Schön J, Abdollahinia A, Müller R, Benick J, Hermle M, Warta W and Schubert M C 2013 Predictive simulation of doping processes for silicon solar cells *Energy Procedia* **38** 312–20